Two-Color Operation in High-Gain Free-Electron Lasers

H. P. Freund
Science Applications International Corporation, McLean, Virginia 22102

P. G. O'Shea
Department of Electrical and Computer Engineering and Institute for Plasma Research, University of Maryland, College Park, Maryland 20742

(Received 8 October 1999)

Two-color operation in free-electron laser (FEL) amplifiers is studied using a 3D nonlinear polychromatic simulation. We assume the FEL is seeded at two closely spaced wavelengths within the gain band, and study the growth of the seeds and a discrete spectrum of beat waves that are outside the gain band. The beat waves grow parasitically due to electron bunching in the seeded waves with growth rates higher than the seeded waves. Injection of narrow-band seeds ensures a discrete spectrum. An example is discussed corresponding to an x-ray FEL; however, the physics is applicable to all spectral ranges.

PACS numbers: 41.60.Cr, 52.75.Ms

Two-color operation of free-electron lasers (FELs) at closely spaced wavelengths is of considerable interest. Applications exist over a broad range of wavelengths involving pump-probe experiments [1], multiple wavelength anomalous scattering [2], or any process where there is a large change in cross section over a narrow wavelength range [3]. Previous demonstrations of two-color operation have used low gain, infrared oscillators, and fall into two categories: (1) pulse switching mode, and (2) segmented undulator. In the pulse switching two-color FEL [4], two different undulators are used and the switching rate is typically on the order of 10 Hz between wavelengths. The alternative scheme involves using a two-segment undulator [5] with different gap and undulator parameters allowing simultaneous operation at two wavelengths.

In this paper we consider simultaneous operation of a high-gain FEL amplifier at two wavelengths using a single-segment undulator and narrow-band seed lasers at two closely spaced wavelengths within the FEL gain band. Each seed is assumed to have a bandwidth much less than the FEL gain bandwidth. Because the seeds can be controlled independently, two-color operation can occur not only simultaneously, but also sequentially in any temporal combination determined by the switching mode of the seeds and the electron beam pulse structure. Both colors will travel along the same path at the FEL exit. For some applications this feature may be undesirable; however, the colors can be separated using dispersive elements.

Our purpose is to study the dynamics of two-color operation in seeded high-gain FEL amplifiers where the gain length is much less than the undulator length. Because cavity mirrors are unnecessary, high-gain FELs have much greater wavelength flexibility than low-gain oscillators. The specific example considered is that of an x-ray FEL with parameters corresponding to the Linac Coherent Light Source (LCLS) at the Stanford Linear Accelerator Center [6]; hence, the analysis has implications for future fourth generation light sources. X-ray lasers are not available at the wavelengths of interest for the LCLS; however, an alternate scheme for generating the seeds is possible that relies on a proposal [7] in which the undulator is broken into two segments. X rays across the entire FEL gain band are generated in the first segment by the amplification of noise (the so-called SASE or self-amplified spontaneous emission process). As proposed [7], the SASE emission is then passed through a monochromator whose narrow-band output is then reintroduced in synchronism with the electron beam in the second undulator segment. This proposal can be generalized to include a pair of monochromators that would select two wavelengths within the FEL gain band. It should be emphasized, however, that the basic physical mechanism is relevant to FEL operation in all spectral ranges, and applications to two-color experiments in the infrared (where seed lasers are available) may be of equal or greater interest.

The intermodulation of the electron beam by the two seeded waves results in a nonlinear interaction that generates a discrete spectrum of beat waves extending beyond the FEL gain band, and which have growth rates higher than that of the seeded waves. This is a well-known phenomenon in traveling wave tubes used in communications [8] that operate by a similar axial bunching mechanism, where the intermodulation between multiple signals results in unwanted nonlinearities. While these nonlinearities may or may not be important in FELs, the effects on the output spectrum are important and must be considered.

The 3D nonlinear, polychromatic simulation code MEDUSA [9,10] is used to simulate the nonlinear interaction of two narrow-band, closely spaced driven signals. MEDUSA employs planar wiggler geometry and treats the electromagnetic field as a superposition of Gauss-Hermite modes using a source-dependent expansion [11]. The field equations are integrated simultaneously with the 3D Lorentz force equations for an ensemble of electrons. No wiggler average is imposed on the orbit equations. The electromagnetic field is represented by a polychromatic

superposition of Gauss-Hermite modes in harmonics of ω_0 in the form

$$\delta\mathbf{A}(\mathbf{x},t) = \hat{\mathbf{e}}_x \sum_{l,n,h} e_{l,n,h}(x,y)\,[\delta A^{(1)}_{l,n,h}\cos\varphi_h + \delta A^{(2)}_{l,n,h}\sin\varphi_h]. \quad (1)$$

Here h denotes the frequency harmonic, and $\varphi_h = h(k_0 z - \omega_0 t) + \alpha_h r^2/w_h^2$ is the vacuum phase, where $k_0 = \omega_0/c$, w_h is the spot size, and α_h denotes the phase front curvature. The transverse structure is described by $e_{l,n,h}(x,y) = \exp(-r^2/w_h^2)H_l(\sqrt{2}\,x/w_h)H_n(\sqrt{2}\,y/w_h)$ and H_l is the Hermite polynomial of order l and of the hth harmonic. The amplitudes $\delta A^{(1,2)}_{l,n,h}$, as well as w_h and α_h, are assumed to vary more slowly than the wavelength. The dynamical equations are

$$\left(\frac{d}{dz} + \frac{w_h'}{w_h}\right)\begin{pmatrix}\delta a^{(1)}_{l,n,h}\\ \delta a^{(2)}_{l,n,h}\end{pmatrix} + K_{l,n,h}\begin{pmatrix}\delta a^{(2)}_{l,n,h}\\ -\delta a^{(1)}_{l,n,h}\end{pmatrix} = \begin{pmatrix}s^{(1)}_{l,n,h}\\ s^{(2)}_{l,n,h}\end{pmatrix}, \quad (2)$$

where $\delta a^{(1,2)}_{l,n,h} = e\,\delta A^{(1,2)}_{l,n,h}/m_e c^2$, the "prime" superscript denotes a z derivative, and

$$K_{l,n,h} = (l+n+1)\left(\alpha_h\frac{w_h'}{w_h} - \frac{\alpha_h'}{2} - \frac{1+\alpha_h^2}{hk_0 w_h^2}\right), \quad (3)$$

$$\begin{pmatrix}s^{(1)}_{l,n,h}\\ s^{(2)}_{l,n,h}\end{pmatrix} = \frac{2\omega_b^2}{h\omega_0 c}\,\frac{1}{2^{l+n}l!\,n!\,w_h^2}\left\langle\frac{v_x}{|v_z|}\,e_{l,n,h}\begin{pmatrix}\cos\varphi_h\\ -\sin\varphi_h\end{pmatrix}\right\rangle, \quad (4)$$

where $\omega_b^2 = 4\pi e^2 n_b/m_e$ for a beam density n_b, and v_x and v_z are the particle velocities in the x and z directions. For Gaussian energy and phase space distributions, the source terms are

$$\langle(\cdots)\rangle = \int_0^{2\pi}\frac{d\psi_0}{2\pi}\int_0^\infty d\gamma_0\,\frac{\exp[-(\gamma_0-\overline{\gamma}_0)^2/2\Delta\gamma^2]}{\sqrt{\pi/2}\,\Delta\gamma[1+\mathrm{erf}(\overline{\gamma}_0/\sqrt{2}\,\Delta\gamma)]} \times\int\!\!\int\!\!\int\!\!\int dx_0\,dy_0\,dp_{x0}\,dp_{y0}\,\frac{\exp(-r_0^2/2\sigma_r^2 - p_{\perp 0}^2/2\sigma_p^2)}{(2\pi)^2\sigma_r^2\sigma_p^2}(\cdots), \quad (5)$$

where the average is over the initial beam parameters (denoted by the subscript "0") in phase (ψ_0), energy (γ_0), and phase space (x_0, y_0, p_{x0}, p_{y0}), $\overline{\gamma}_0$ and $\Delta\gamma$ denote the average energy and the energy spread, and σ_r and σ_p describe the phase space parameters.

The diffraction of each harmonic component in the SDE is governed by

$$\frac{w_h'}{w_h} = \frac{2\alpha_h}{hk_0 w_h^2} - Y_h, \quad (6)$$

$$\frac{\alpha_h'}{2} = \frac{1+\alpha_h^2}{hk_0 w_h^2} - (X_h + \alpha_h Y_h), \quad (7)$$

where X_h and Y_h are defined in terms of the source terms as

$$X_h = 2\,\frac{(s^{(1)}_{2,0,h} + s^{(1)}_{0,2,h})\delta a^{(2)}_{0,0,h} - (s^{(2)}_{2,0,h} + s^{(2)}_{0,2,h})\delta a^{(1)}_{0,0,h}}{\delta a^2_{0,0,h}}, \quad (8)$$

$$Y_h = -2\,\frac{(s^{(1)}_{2,0,h} + s^{(1)}_{0,2,h})\delta a^{(1)}_{0,0,h} + (s^{(2)}_{2,0,h} + s^{(2)}_{0,2,h})\delta a^{(2)}_{0,0,h}}{\delta a^2_{0,0,h}}, \quad (9)$$

and $\delta a^2_{0,0,h} = \delta a^{(1)2}_{0,0,h} + \delta a^{(2)2}_{0,0,h}$. Vacuum diffraction is recovered by Eqs. (6)–(9) when $X_h = Y_h = 0$ yielding $w_h = w_h(z=0)[1 + z^2/z_{0h}^2]^{1/2}$, $\alpha_h = z/z_{0h}$, and $z_{0h} = hk_0 w_h^2(z=0)/2$ is the Rayleigh range.

If ω_1 and ω_2 denote the frequencies of the two seeded waves ($\omega_2 > \omega_1$), then ω_0 is chosen so that $\omega_1 = N_1\omega_0$ and $\omega_2 = N_2\omega_0$ where N_1 and N_2 are integers. Since ω_1 and ω_2 must be closely spaced for both waves to be within the gain band, N_1 and N_2 are typically much greater than unity. Nonlinear intermodulations between the two waves are possible, and we must also include a spectrum of beat waves separated from the seeded waves in frequency by harmonics of $\Delta\omega = \omega_2 - \omega_1$. In practice this spectrum must be truncated, and we include only the two nearest neighbor beat waves above and below the seeded waves. Similar beat waves are also found in traveling wave tube amplifiers used in communications [11]. The beat waves at $2\omega_2 - \omega_1$ and $2\omega_1 - \omega_2$ ($3\omega_2 - 2\omega_1$ and $3\omega_1 - 2\omega_2$) are referred to as third (fifth) order intermodulation products. Since the beat waves are generated by nonlinear interactions between the driven waves, the intermodulation products grow rapidly. For driven signals with comparable growth rates, the gain lengths of the nth order intermodulation products scale as $1/n$ times the gain lengths of the seeded waves. This is similar to the scaling found in the nonlinear generation of harmonics in FELs [9]. While these beat waves have important implications on the linearity of the traveling wave tube amplifiers, the issue of linearity is not of prime importance in fourth generation light sources. However, the saturated powers in the seeded waves and their intermodulation products are of interest.

The parameters under consideration correspond to the LCLS [6]. The electron beam has a 14.35 GeV energy, a 3400 A peak current, a normalized emittance of 1.5π mm mrad, and an energy spread of 0.02%. The peak, on-axis wiggler field strength is 13.2 kG with a period of 3.0 cm. We consider a matched electron beam that has been shown to result in the optimal growth rate [12]; hence, the phase space parameters are $\sigma_r = \sqrt{\beta\varepsilon/\overline{\gamma}_0}$ and $\sigma_p = m_e c\sqrt{\overline{\gamma}_0\varepsilon_n/\beta}$, where ε_n is the normalized emittance and $\beta = \overline{\gamma}_0/a_w k_w$ is the beta function. The resonance wavelength for these parameters is in the vicinity

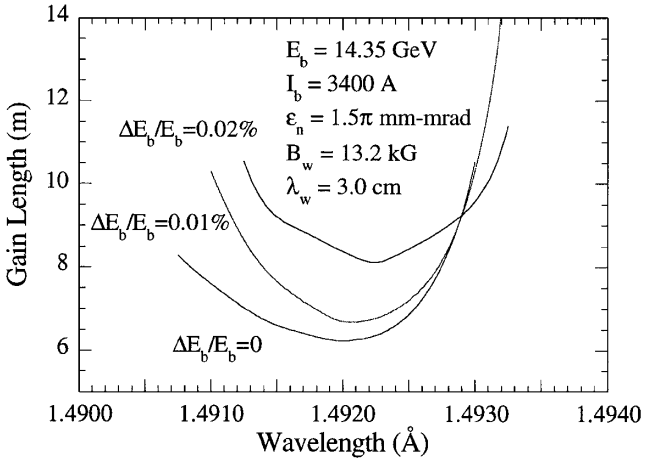

FIG. 1. The gain length versus wavelength.

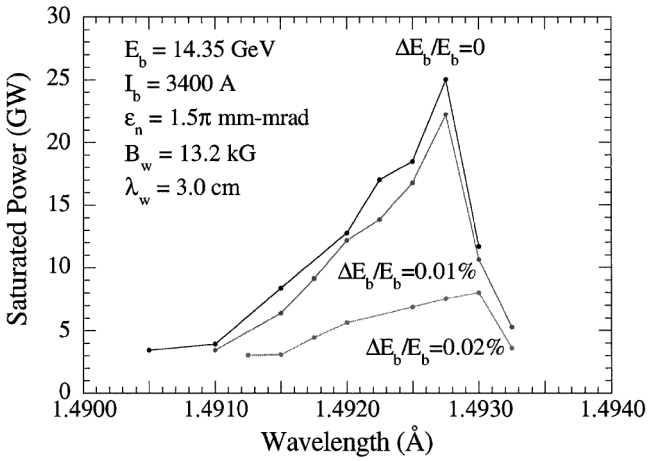

FIG. 2. The saturated power versus wavelength.

of 1.5 Å. While the LCLS employs a multisegment wiggler design, we choose for simplicity to employ a single segment, parabolic-pole-face wiggler model in the analysis. This presents no handicap, however, since the present analysis is not a detailed design study. A seeded FEL requires drive powers in excess of the spontaneous synchrotron radiation. The LCLS beam is estimated to emit approximately 44 W of spontaneous power per gain length into the dominant mode [13]; hence, the seeded waves require powers of the order of several kW.

A characterization of single-color seeded amplifier performance is a necessary prelude to the multicolor analysis. A plot of the gain length versus wavelength is shown in Fig. 1 for a vanishing energy spread and for energy spreads of 0.01% and 0.02%. As shown, the minimum gain length and the corresponding wavelength varies with energy spread over the range of 6.21–8.04 m and 1.4920–1.4922 Å, respectively. The gain band itself extends over the range of $\Delta\omega/\omega \approx 0.15\%$. The saturated power is plotted versus wavelength in Fig. 2 for the same choices of energy spread. The saturated power depends sensitively on both the energy spread and the wavelength. Indeed, the maximum saturated power decreases from about 25 GW for a vanishing energy spread to 22 GW when the energy spread is 0.01% and finally to about 8 GW for an energy spread of 0.02%. It is clear from Figs. 1 and 2 that the gain length (saturated power) increases (decreases) rapidly as the energy spread increases from 0.01% to 0.02%. As a consequence, it is important to keep the energy spread below about 0.02% for the LCLS to operate near optimal efficiency.

We now consider two driven waves with wavelengths of 1.4918 and 1.4925 Å, as well as the two nearest neighbor beat waves at 1.4911, 1.4933, 1.4903, and 1.4940 Å. For the sake of convenience, we assume that the seeded powers are 300 kW. This is well beyond what is required for the driven signals to overwhelm the spontaneous emission, and ensures that the interaction length in simulation is sufficiently short that computer run times are not excessive. We chose these two seed wavelengths without loss of generality. If we had chosen a different pair within the gain band, the results would be quantitatively similar, except that the spacing of the beat waves would be altered. Note that, as shown in Fig. 1, with an energy spread of 0.02% the beat waves are outside the FEL gain band and would not normally grow without the nonlinear beating of the seeded waves. The evolution of the seeded waves and the intermodulation products are shown in Fig. 3.

The gain lengths and saturated powers for the various waves in the simulation are summarized in Table I. The gain lengths for the two seeded waves of 9.373 m (1.4918 Å) and 9.013 m (1.4925 Å) correspond to the gain lengths shown in Fig. 1 for a monochromatic seed. However, the saturated powers for the driven waves are somewhat lower as would be expected in the case of the simultaneous growth of two waves. The interesting feature is the growth of the beat waves. If Γ_1 and Γ_2 denote the growth rates for the seeded waves, then the third (fifth) order intermodulation products will have growth rates of $2\Gamma_1 + \Gamma_2$ and $2\Gamma_2 + \Gamma_1$ ($3\Gamma_1 + 2\Gamma_2$ and $3\Gamma_2 + 2\Gamma_1$),

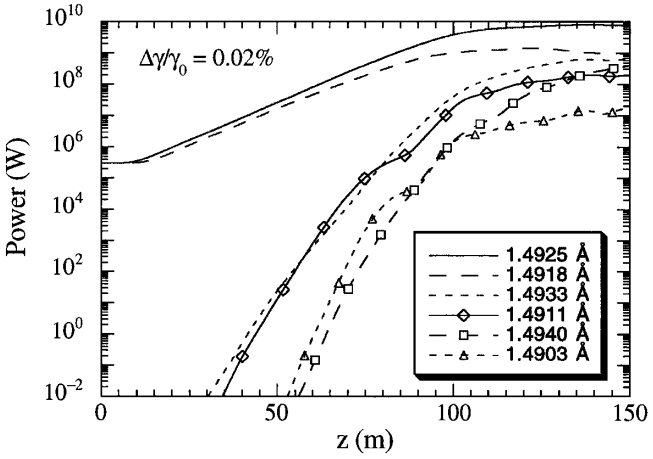

FIG. 3. Evolution of the power in the seeded waves and the beat waves.

TABLE I. Gain lengths and saturated powers for the seeded and beat waves.

Wavelength (Å)	Gain length (m)	Saturated power
1.4903	1.727	14.4 MW
1.4911	2.459	198 MW
1.4918	9.277	1.03 GW
1.4925	8.982	8.02 GW
1.4933	3.106	636 MW
1.4940	1.755	227 MW

and this is approximately reproduced in the simulation results. Observe that if $\Gamma_1 = \Gamma_2$ then the gain length of the nth order scales as $1/n$ times the gain length of the seeded waves.

The scaling of the beat wave growth rates can be illustrated mathematically by noting that the seeded waves nonlinearly give rise to an oscillatory current. If the electric field of the seeded waves is $E_{\text{seed}} = E_1(z)\cos(k_1 z - \omega_1 t) + E_2(z)\cos(k_2 z - \omega_2 t)$, then the beating of these waves drives a nonlinear current

$$J_{\text{NL}} = \sum_{k,l=1}^{2} \sum_{m,n=1}^{\infty} \sigma^{(\text{NL})}_{k,l,m,n} E_k^m E_l^n \times \cos^m(k_k z - \omega_k t)\cos^n(k_l z - \omega_l t), \quad (10)$$

where $\sigma^{(\text{NL})}$ describes the nonlinear conductivity whose detailed form is not required to obtain the scaling law. The third order intermodulation products arise from the terms in $E_1^2 E_2^1$ and $E_1^1 E_2^2$ that yield oscillatory components varying in frequency as $2\omega_1 - \omega_2$ and $2\omega_2 - \omega_1$. These components of J_{NL} generate the third order intermodulation products which, if $E_1 \approx \exp(\Gamma_1)$ and $E_2 \approx \exp(\Gamma_2)$, have growth rates of $2\Gamma_1 + \Gamma_2$ and $2\Gamma_2 + \Gamma_1$.

The power levels achieved by the intermodulation products are substantial. The beat waves exhibit a complex variation with axial position reflecting the details of the bunching process, and the beat waves saturate at different positions. This makes a detailed comparison of the power levels difficult. However, at the saturation point of the fastest growing driven wave (i.e., $z = 138$ m), the third (fifth) order intermodulation products achieve peak power levels of 636 and 227 MW (198 and 14.4 MW). It is evident that while the driven waves are dominant, the beat waves exhibit substantial power levels, and must be taken into account in any two-color experiment.

It should be noted that the power level attained by the 1.4925 Å seed is comparable to that found in the single-wavelength limit shown in Fig. 2, while the power attained by the 1.4918 Å seed is much lower. Note that the growth rates in the linear, exponentially growing regime for the two seeds are identical to that found for each in the single-wavelength limit. However, the 1.4925 Å seed has the higher growth rate and saturates before the 1.4918 Å seed, thereby suppressing the saturated power of the second seed.

In summary, we have considered two-color operation in high-gain FEL amplifiers, and used a 3D nonlinear polychromatic simulation code to study the phenomenon. The growth of two seeded waves with closely spaced wavelengths within the FEL gain band was analyzed along with a discrete spectrum of beat waves (that are not within the gain band) and grow parasitically due to the bunching caused by the seeded waves. For the x-ray FEL example presented, the beat waves are found to grow rapidly and to reach substantial power levels; hence, the presence of these beat waves must be considered in any two-color experiment. We reiterate that while an x-ray example has been presented the basic physical mechanism is relevant to FEL operation in all spectral ranges, and applications to two-color experiments in the infrared may be of equal or greater interest.

The computational work was supported by Science Applications International Corporations Advanced Technology Group under IR&D Subproject No. 01-0060-73-0890-000.

[1] R. Prazeres *et al.*, Nucl. Instrum. Methods Phys. Res., Sect. A **407**, 464 (1998).
[2] J. Drenth, *Principles of Protein X-ray Crystallography* (Springer-Verlag, New York, 1999), 2nd ed.
[3] E. Johnson (private communication).
[4] T. I. Smith *et al.*, Nucl. Instrum. Methods Phys. Res., Sect. A **407**, 151 (1998).
[5] D. A. Jaroszynski *et al.*, Phys. Rev. Lett. **72**, 2387 (1994).
[6] M. Cornacchia *et al.*, Proc. SPIE Int. Soc. Opt. Eng. **2988**, 5 (1997).
[7] J. Feldhaus, E. L. Saldin, J. R. Schneider, E. A. Schneidmiller, and M. V. Yurkov, Opt. Commun. **140**, 341 (1997).
[8] A. S. Gilmour, Jr., *Principles of Traveling Wave Tubes* (Artech House, Boston, 1994).
[9] H. P. Freund and T. M. Antonsen, Jr., *Principles of Free-electron Lasers* (Chapman & Hall, London, 1996), 2nd ed.
[10] H. P. Freund, S. G. Biedron, and S. V. Milton, IEEE J. Quantum Electron. **36**, 275 (2000).
[11] P. Sprangle *et al.*, Phys. Rev. Lett. **59**, 202 (1987); Phys. Rev. A **36**, 2773 (1987).
[12] H. P. Freund and P. G. O'Shea, Phys. Rev. Lett. **80**, 520 (1998).
[13] M. Xie, in *Proceedings of the IEEE 1995 Particle Accelerator Conference* (IEEE, New York, 1995), p. 183 [IEEE Cat. No. 95CH35843].